JOURNAL OF SYNCHROTRON RADIATION
ISSN 1600-5775

Visualization of woven bone structure through analysis of biopsy specimens using synchrotron radiation and conventional X-ray microcomputed tomography

Seung-Jun Seo[a] and Yong-Gun Kim[a,b]*

[a]Department of Periodontology, School of Dentistry, Kyungpook National University, Daegu 41940, Republic of Korea, and [b]Institute for Translational Research in Dentistry (ITRD), Kyungpook National University, Daegu 41940, Republic of Korea. *Correspondence e-mail: periokyg@knu.ac.kr

Received 6 March 2019
Accepted 11 November 2019

Edited by P. A. Pianetta, SLAC National Accelerator Laboratory, USA

Keywords: synchrotron radiation X-ray μCT; conventional X-ray μCT; woven bone; bone biopsy.

This study explores the application of synchrotron radiation and conventional microcomputed tomography (SR-μCT and C-μCT, respectively) in evaluating bone-biopsy specimens. Bone-biopsy specimens were obtained using a trephine bur during bone-graft removal for implant placement six months after performing a maxillary sinus bone-graft procedure. Image data of specimens were obtained using SR-μCT and C-μCT. SR-μCT was performed using the 6C biomedical imaging beamline at the Pohang Accelerator Laboratory with a monochromatic X-ray beam of 23 keV, and C-μCT was performed using a table-top CT scanner (Skyscan 1272). Reconstruction images obtained using the two methods were qualitatively compared with 2D images evaluated under 3D visualization. The SR-μCT images, especially of the new-bone–graft–woven-bone formation, were less noisy and sharper than the C-μCT images. To evaluate the new-bone–graft–woven-bone formation, only the SR-μCT images showed areas of new bone (NB) formation with bone substitute (BS; Bio-Oss) and woven bone (WB) contact, and correctly visualized true 3D structures of bone formation. Hence, μCT techniques are non-destructive and can provide detailed images of bone biopsy. In particular, SR-μCT can be used to obtain improved image quality with contrast of NB, BS and WB, demonstrating a level of detail comparable with bone formation. SR-μCT could be an unbiased 3D alternative for imaging WB formation and for high-throughput analysis.

1. Introduction

The purpose of bone regeneration in medicine is to restore and maintain the lost function of bones. In the dental field, alveolar bone lost due to tooth loss or periodontal disease is regenerated through bone grafting (Finkemeier, 2002). The clinical success of bone regeneration is achieved through tissue analysis and measurement, and the accurate evaluation of the bone healing is important (Kulak & Dempster, 2010). Microanalysis of biomaterials and biologically regenerated tissues is essential for the accurate assessment of bone healing.

The key aspects of microanalytic tools are image quality (high-quality histological sections), resolution (labeling fluorochromes) and accuracy. Bone-biopsy samples contain information on bone regeneration and remodeling along with their complex structure (Kulak & Dempster, 2010). The amount of biopsy tissue [including new bone (NB) with graft materials and soft tissue] after a surgical treatment of maxillary sinus floor elevation (MSFE) has been observed and estimated (Yildirim *et al.*, 2001). Among the current methods to analyze biopsy tissue in general, the hematoxylin-eosin

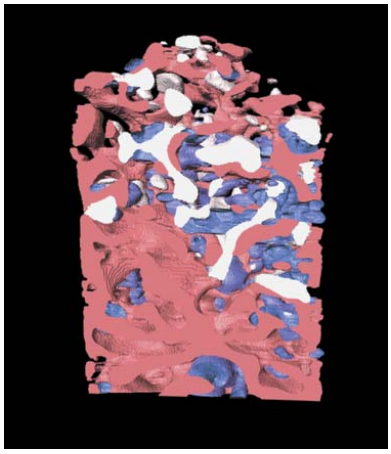

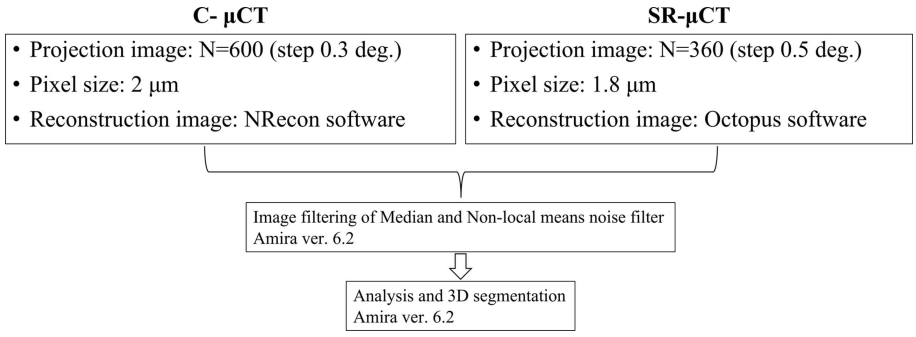

Figure 1
Image-processing diagrams.

staining method is the most widely used histological technique (Froum *et al.*, 2008; Jensen & Sennerby, 1998). Histological techniques are exceptionally useful in highlighting biological structures but they involve long pre-processing and sectioning of the sample, which may create deformation. On the other hand, the analysis of information for bone dynamics is only for the longitudinal direction view and uses a limited number of sections.

Avoiding the demerits of conventional histomorphometry, microcomputed tomography is a non-destructive imaging technique. It is used in the bone analyses of animal models, such as bone growth, remodeling and regeneration (Irie *et al.*, 2018). Microcomputed tomography (μCT) has been previously used in bone biopsy to visualize and analyze NB formation with bone substitute (BS) (Stelzle & Benner, 2010; Klein *et al.*, 2013; Trisi *et al.*, 2006). However, the demerits of μCT images are noise, artifacts and low-contrast resolution (Bouxsein *et al.*, 2010). This poses a hurdle for its ability to visualize soft tissues of low density, which makes segment separation of hard tissue from soft tissue difficult without using histological sections as references.

Despite the continued development of analytical equipment, analysis using tissue staining is still in use. It is impossible to make measurements in three dimensions using the method of tissue staining, but it is accurate, based on analysis and evaluation at the cellular and molecular levels.

The use of synchrotron radiation X-ray μCT (SR-μCT) can potentially solve these shortcomings and yield a high-resolution 2D/3D image. The advantage of this approach compared with conventional μCT (C-μCT) is that using it with a highly collimated and parallel monochromatic beam eliminates beam-hardening artifacts. The photon flux is several orders of magnitude higher than the conventional X-ray tube sources. This collimated beam gives an increased spatial resolution for the accurate measurement of tissue-mineral density. The additional advantage of using this method is that beams pass through dense structures effectively, making internal structures visible. SR-μCT has been used for a precise volume analysis of NB, BS (Seo *et al.*, 2015) and trabecular bone architecture (Martín-Badosa *et al.*, 2003) in the bone biopsy of humans and, recently, to investigate genetic variations in the mineral density and microstructural properties of murine cortical bone, including the vascular canals and osteocyte lacunae (Raum *et al.*, 2007; Schneider *et al.*, 2007).

Unlike conventional absorption-based imaging techniques, phase-contrast imaging has been widely used to improve soft-tissue contrast as the phase shift varies with materials of different X-ray refractive indices (Raven *et al.*, 1996). This phase shift is observed at the edges of structures, enhancing the contrast when the X-ray absorption is mainly of low contrast. High-contrast images make it easier to apply threshold methods such as segmentation and analysis. However, X-ray CT images still exhibit motion artifacts and are noisy. Possible solutions include the correction of beam hardening, the removal of motion artifacts, mitigation by high-resolution CT and the implementation of a density-based threshold method. Pre-processing steps improve the output image when included before segmentation (Bouxsein *et al.*, 2010). Therefore, to obtain a higher-quality output, pre-processing is necessary for X-ray CT imaging.

This study aimed to provide an enhanced image contrast and a threshold approach to quantify a bone-biopsy sample using high-resolution μCT. The specific aims were (i) to investigate the effects of image contrast and the pre-processing filtering method on segmentation measurements of SR-μCT and C-μCT (Fig. 1); and (ii) to demonstrate the segmentation that can be used for high-resolution microstructure and high-throughput analysis of NB, BS and woven bone (WB).

2. Materials and methods

2.1. Sample preparation

Ethical approval for this study was obtained from the Ethics Committee, Kyungpook National University Hospital Institutional Review Board. Informed consent was obtained from the patient, and the biopsy sample was from a partially edentulous patient with at least the posterior upper tooth missing. With the surgeon using the lateral approach, after flap elevation an osteotomy on the lateral wall of the maxilla was performed to create a window. The space created between the maxillary alveolar process and the elevated Schneiderian membrane was filled using BS (Bio-Oss, Geistlich Pharma AG, Wolhusen, Switzerland). To avoid infection, the patient received Augmentin (625 mg), Etodin (200 mg) and Stilen (60 mg) daily over a seven day period. After six months of uneventful healing, the implant sites were prepared with

trephine burs (3.0 mm outer diameter and 2.0 mm inner diameter) to obtain bone cores (vertical biopsies). The bone specimen was fixed in 4% neutral-buffered paraformaldehyde for use in SR-μCT and C-μCT investigations. In the analysis, the dimensions of the bone specimen were ∼3 mm (height) × 2 mm (diameter) for SR-μCT and 6 mm (height) × 2 mm (diameter) for C-μCT in the grafted area.

2.2. Conventional μCT acquisition

Conventional μCT scanning was performed using a table-top μCT scanner (Skyscan1272, Bruker, Belgium). This scanner consists of an X-ray tube with a current of 200 μA, a source voltage of 50 kVp and no filter. We used an exposure time of 200 ms and a rotation step of 0.3° over 180°. This resulted in an image pixel size of 2 μm.

2.3. SR-μCT acquisition

The SR-μCT scans were performed at the 6C Biomedical Imaging (BMI) beamline of the Pohang Light Source, Pohang City, South Korea (PLS-II), which has an electron energy of 3.0 GeV and a stored current of 350 mA in top-up mode. This beamline provided a monochromatic beam of relatively large spectral bandwidth ($\Delta E/E$) of 1–2% using multilayered crystals. The multilayered crystals were coated with tungsten and boron carbide bilayers (Incoatec, Germany). The default beam size of the 6C beamline is 100 μm and it delivers a photon flux of 10×10^{11} photons s^{-1} mm^{-2}. The sample was scanned using a monochromatic X-ray beam energy of 23 keV. The images were acquired using a charge-coupled-device (CCD) camera (Zyla, Andor, UK) system, which consisted of a fluorescent screen (YAG:Ce, thickness 50 μm, Crytur, Czech) that converts monochromatic X-rays into visible light on the object lens (×4). The field of view was 4.2 mm × 3.0 mm with an effective pixel size of 1.8 μm. The sample-to-detector distance was set to 20 cm. For the tomographic scan, 360 projection images were taken, with an exposure time of 200 ms, each at 0.5° during the rotation of the sample from 0 to 180°. The beamline layout is shown in Fig. 2.

2.4. Image reconstruction

SR-μCT reconstruction was performed using the commercial software *Octopus* (version 8.9; Inside Matters, Aalst, Belgium). The process was as follows: removal of white spots, normalization, ring filtration, phase filtering (modified Bronnikov algorithm), sinogram creation. It implemented the ordinarily filtered back-projection algorithm. The resulting images mapped the local X-ray attenuation coefficient and the boundaries enhanced by the interference of the transmitting coherent X-rays. C-μCT reconstruction was performed using the *NRecon* software provided by the scanner manufacturer (version 1.6.9; Skyscan, Kontich, Belgium).

2.5. Measurement of mean contrast value

After normalized images of 0 to 255 gray level intensities were exported to reconstruction images, intensity profiles of bone formation (BF) were qualitatively evaluated via the plotting of a line profile. Changes along the line between the NB, BS and WB corresponded to variations in the intensity. The mean contrast value of BF was quantitatively assessed by calculating the contrast-to-noise ratio (CNR) using the following formula (Bushberg *et al.*, 2003),

$$\mathrm{CNR} = \frac{\mathrm{IBF} - \mathrm{IBG}}{\sigma \mathrm{BG}},$$

where IBF is the maximum intensity value for the BF and IBG is the minimum intensity value from an equal size area (5 pixels × 5 pixels) enclosing the entire background area (BG). σBG is the standard deviation of the intensity values in the background image. The selections of equal sizes used for calculating IBF, IBG and σBG were outlined in slices clearly separating the NB, BS and WB measurements of 12 slices.

2.6. Image segmentation and analysis

For 3D image visualization as well as processing and analysis, another commercial software, *Amira* (version 6.2; FEI Co., Hillsboro, OR, USA), was used. The noise reduction was median filtered and smoothened with the software's non-local means noise (NLMF) filter function on the reconstruction images. The volume analysis (see Table 1) was preceded by image segmentation. The individual pixels of the 3D images were classified into the categories NB, BS and WB. The gray levels in a single segment fluctuated, often exceeding the threshold values set to discriminate between the different categories. In order to suppress the noise, we applied the NLMF filtration algorithm. The same procedure was successfully applied for the C-μCT 3D image sets. 2D area

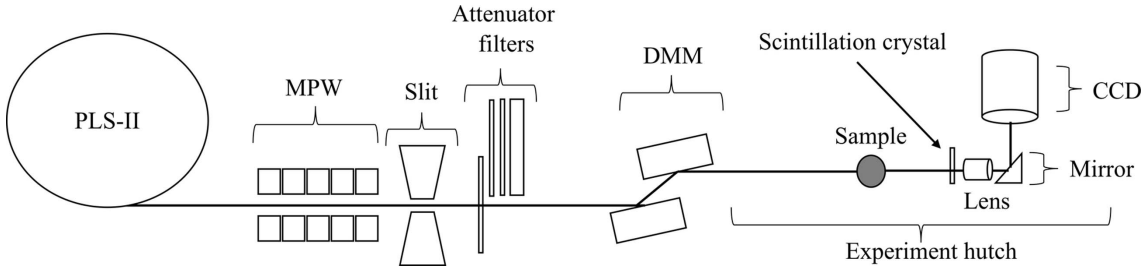

Figure 2
Layout of the SR-μCT experiment performed using the 6C BMI beamline at PLS-II. A 23 keV monochromatic beam from a double multilayer monochromator (DMM) attenuated by a graphite attenuator was used. The beam propagated 20 cm from the bone-biopsy sample to a scintillation crystal (YAG:Ce, thickness 50 μm) that converted the monochromatic X-rays into visible light on an object lens (×4).

Table 1
Results obtained from the volume analysis of SR-μCT and C-μCT.

	NB (mm^3)	BS (mm^3)	WB (mm^3)	Total (mm^3)
SR-μCT	3.54	1.61	1.6	6.75
C-μCT	3.02	1.29	—	4.31

analysis of each bone material was performed using the following formula (Seo *et al.*, 2015): Area percentage per slice (%) = $N \times$ Pixels (width $\times$ height) $\times$ $1/\pi r^2 \times 100$, and the ratio and distribution of NB and BS were measured every 8 μm from the specimen. The volume analysis was conducted by counting the number of pixels belonging to each category.

3. Results

3.1. Improvement of image quality and contrast

Fig. 3 presents the sliced images of the bone-biopsy specimen harvested before implant placement in the graft area. The images obtained by SR-μCT and C-μCT were compared using the reconstruction program *Octopus*, version 8.9 (Inside Matters, Aalst, Belgium). As shown in Figs. 3(*a*) and 3(*d*), some of the main characteristics of the bone-graft fractions appear lighter and the NB appears denser, and soft tissues are invisible, including the WB region. The sliced images differentiated the two major constituents of contrast quite well, *i.e.* the NB and BS material Bio-Oss. However, a number of lower-contrast issues were identified in the C-μCT image compared with the SR-μCT image due to the beam-hardening effect and the ring noise.

To distinguish between the main characteristics of the bone graft fractions possibilities, noise reduction was carried out. Figs. 3(*b*) and 3(*e*) show high-contrast images with the main characteristics of NB, bone graft and WB. The WB was observed by both SR-μCT and C-μCT. The image quality was quantitatively evaluated by plotting the intensity profiles along a horizontal line, *i.e.* the yellow dashed line in Figs. 3(*b*) and 3(*d*). The results in Fig. 3(*c*) of the SR-μCT image at the peak point are robust and sharp. The C-μCT image intensity was of high value (same as the graft material) at the beginning and at the end point due to the beam-hardening effect, and the peak point was not as sharp compared with the SR-μCT image intensity [Fig. 3(*f*)].

3.2. Mean contrast values

The mean image-contrast values measured from the SR-μCT images for the NB, bone graft and WB were 105.1 ± 3.78, 164.8 ± 3.19 and 78.5 ± 2.54, respectively, whereas the corresponding values from the C-μCT images were 85.5 ± 2.71, 105.1 ± 4.04 and 42.5 ± 2.01, respectively. Fig. 4 shows the mean values of the contrast difference between background values. A comparison of the results reveals that the contrast values in the SR-μCT images were different in each region while the contrast values in the C-μCT images were larger in the NB and BS regions and smaller in the WB region compared with the threshold limit.

3.3. 3D visualization and analysis for C-μCT

The 3D datasets generated by C-μCT consisted of about 3236 × 3236 × 3114 voxels. The full field of view and spatial

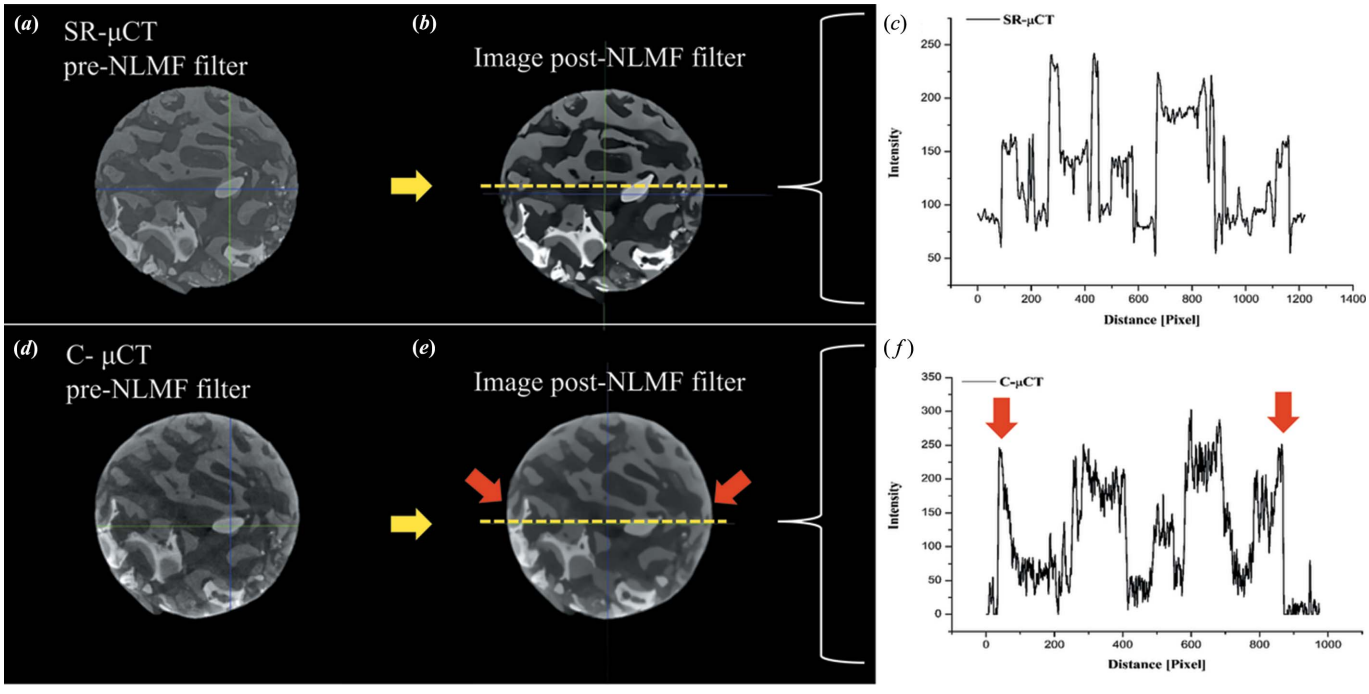

Figure 3
Improved bone-biopsy cross-sectional view in SR-μCT images compared with C-μCT images. (*a*) and (*d*) The reconstruction original images, (*b*) and (*e*) after NLMF filtering, (*c*) and (*f*) intensity line profiles corresponding to the yellow lines shown through the images. The C-μCT images and line profile show the beam hardening effect (red arrow).

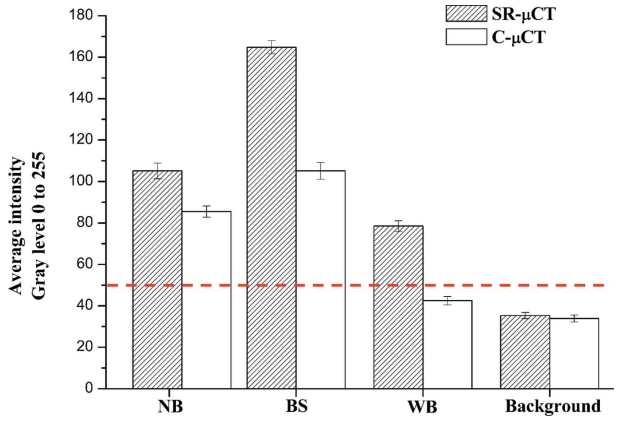

Figure 4
Mean contrast comparison between the SR-μCT and C-μCT images. The limit for applying threshold segmentation is indicated by the red dashed line.

resolution of the C-μCT images allowed a whole-sample segmentation of the NB and BS, as shown in Fig. 5(*a*). The sagittal section shows the inner structure and the NB formation with BS [Fig. 5(*b*)]. The 2D analysis shows a graph of the NB and BS superimposed onto a 3D image background, which was correlated with slice position [Fig. 5(*c*)]. Our results demonstrated that the bone dynamics between NB and BS along the inferior–superior direction after MSFE could be analyzed using 400 slices. The specimen was analyzed in the cross-sectional position and the analysis readily extended over the entire volume. The average volume of the NB and BS measured is summarized in Fig. 5(*d*). The average values were 29.44% and 30.45% for NB formation and 13.39% and 13.07% for BS, giving total values (NB + BS) of 42.83% and 43.52% for SR-μCT and C-μCT, respectively.

3.4. 3D visualization and analysis for SR-μCT

The 3D datasets generated by SR-μCT consisted of about 2379 voxels × 2379 voxels × 2058 voxels. The high-contrast and spatial resolution of the SR-μCT images allowed a robust and sharp segmentation of the NB, BS and WB, as shown in Figs. 6(*a*) and 6(*b*). The 2D analysis shows a graph of the NB, BS and WB superimposed onto a 3D image background, which was correlated with slice position [Fig. 6(*c*)]. Our results demonstrated that the bone dynamics between NB, BS and WB along the inferior–superior direction after MSFE could be analyzed using 400 slices. The specimen was analyzed in the cross-sectional position and the analysis readily extended over the entire volume. The positional variation of the NB and WB fractions clearly indicated the dependence on BS. The average volumes of the NB, BS and WB and the total volume (TV)

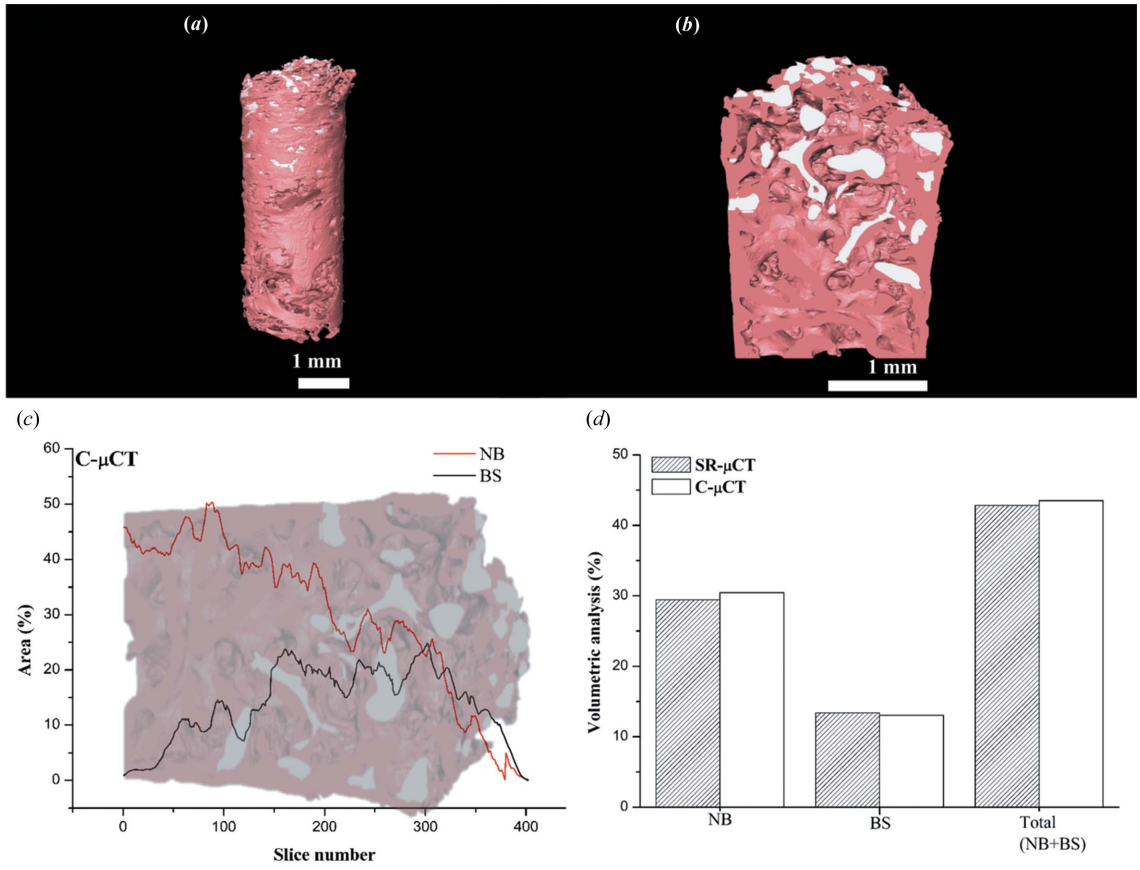

Figure 5
Visualization of the 3D image and analysis of the bone-biopsy specimen acquired by C-μCT. (*a*) A whole bone specimen of a complete segmentation of the NB (red) and BS (white), and (*b*) a sagittal section view. (*c*) Visualization of the 2D analysis of NB and BS in graft sites *versus* slice number, which was correlated with slice position; the background image shows the 3D image of the bone biopsy. (*d*) Comparison of volume analysis between SR-μCT and C-μCT (without WB).

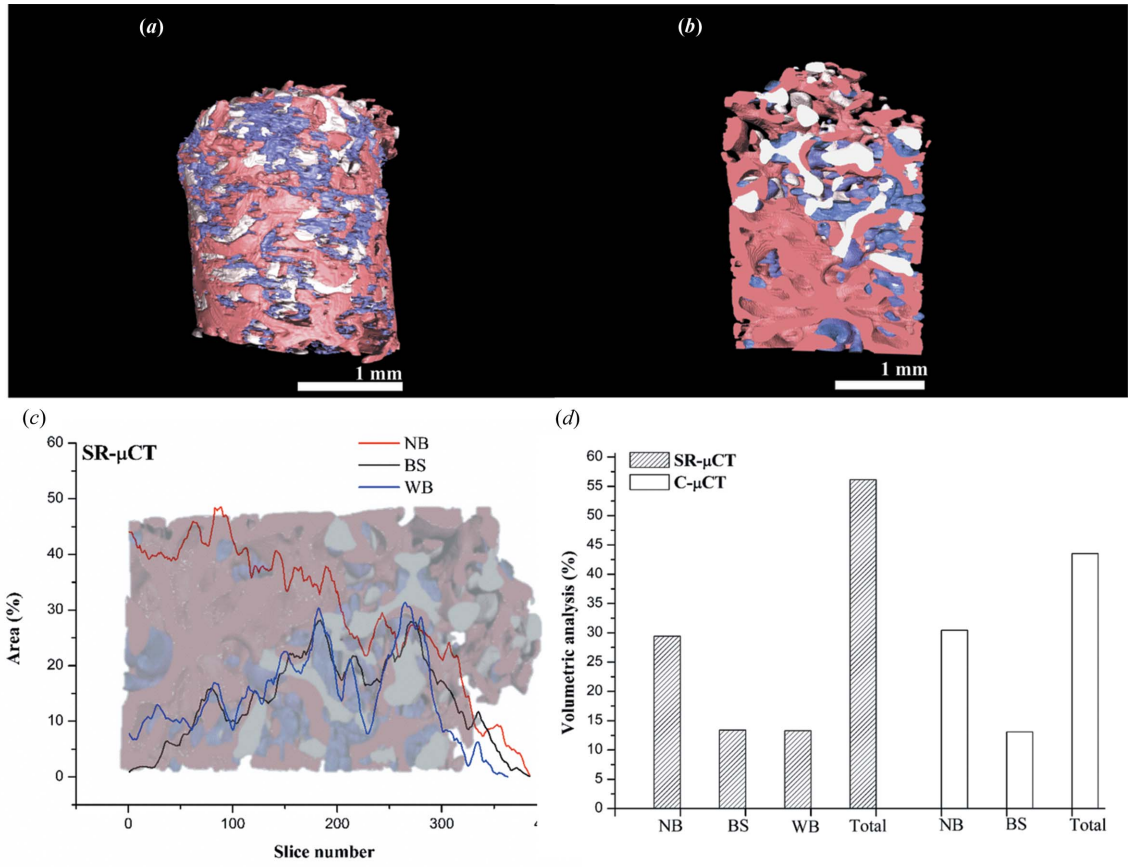

Figure 6
Visualization of the 3D image and analysis of the bone-biopsy specimen acquired by SR-μCT. (*a*) A whole bone specimen of a complete segmentation of the NB (red), BS (white) and WB (purple), and (*b*) a sagittal section view. (*c*) Visualization of 2D analysis of NB, BS and WB in graft sites *versus* slice number, which was correlated with slice position; the background image shows the 3D image of bone biopsy. (*d*) Comparison of volume analysis between SR-μCT and C-μCT.

measured are summarized in Fig. 6(*d*). The average values measured from the SR-μCT data for NB, BS, WB and TV were 29.44, 13.39, 13.29 and 56.12%, respectively. The results suggest that the WB is constantly remodeled by activity via bone regeneration. Previous CT studies revealed the analysis of NB and BS. However, we showed the 3D visualization and analysis of WB. SR-μCT delivers significantly better results than C-μCT because of phase contrast.

3.5. Visualization of WB formation

The high contrast of the SR-μCT images allowed a robust and sharp segmentation of the NB formation, graft material and WB formation using the threshold function in the *Amira* software. Fig. 7(*a*) illustrates a sample of the segmentation results and the corresponding 3D reconstructed model. A clear separation between NB and BS can be seen. The region enclosing the WB is illustrated in the high-quality 3D view in Figs. 7(*b*) and 7(*c*).

4. Discussion

This study is the first work to report on the visualization of a biopsy sample with a WB structure using SR-μCT. In addition, we presented a 3D image obtained by threshold segmentation of the complete NB, BS and WB, and an area or volume analysis. The threshold-segment method presented here can be used to develop the bone analysis of SR-μCT. Results suggest that SR-μCT provides a superior visualization of bone structures over C-μCT.

WB is usually studied via histology, and pre-processing is necessary to create such histological slides. The sample may be damaged in the demineralization process and the results may be distorted in the limited two-dimensional cross-sectional analysis. Previous studies have shown that histomorphometric analysis easily distinguishes between graft particles and surrounding NB, based on staining and morphology (Froum *et al.*, 2008; Jensen & Sennerby, 1998; Yildirim *et al.*, 2001; Moy *et al.*, 1993; John & Wenz, 2004). The analysis in this paper was a quantitative evaluation of 2D images taken from a number of sections for specimens, and the analyzed parameters were for NB, BS and WB regions. We showed that the improved high-contrast SR-μCT images allow for an effective threshold segmentation. The clear and accurate segmentations resulted in a realistic and detailed 3D image of WB structures such as the NB and BS (Fig. 7), and we only assume that these images represented all the elements on the grafted sites.

Recently, for three-dimensional evaluation using μCT, most studies have focused on bone regeneration, and studies of hard tissues or the condition (optics tool, beam condition and

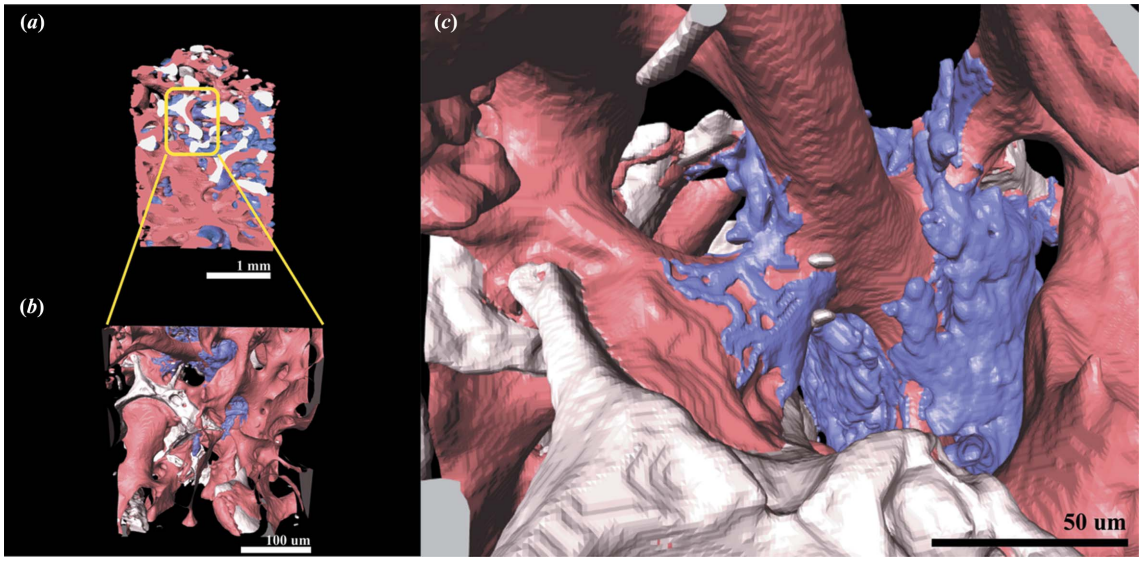

Figure 7
3D visualization image of the bone-biopsy specimen acquired by SR-μCT. (*a*) A whole bone specimen of a complete segmentation of the NB (red), BS (white) and WB (purple), and (*b*) the corresponding high-quality 3D image along with a magnified view (*c*).

image pre-processing) of the WB have not been found. This has been previously assessed only to a limited extent, because weak contrast, such as an unclear boundary due to low absorption coefficient, makes WB invisible on conventional μCT images. Several reports have evaluated NB formation for bone biopsy using C-μCT (Trisi *et al.*, 2006; Klein *et al.*, 2013; Soardi *et al.*, 2014). However, most studies have focused on bone regeneration and analysis of the hard tissues. Soft tissues are more difficult to depict in conventional absorption-based μCT imaging because of low-energy X-ray blocking by attenuation filters, and because WB, with a low absorption coefficient, could not be depicted in the image. In contrast, here we tried not to use a C-μCT attenuation filter in order to utilize the low-energy X-rays. As a result, we observed WB in a 2D image through the image-filter processing and showed the potential to visualize WB. However, it is more difficult to carry out 3D segmentation for WB by C-μCT imaging due to the presence of fine low-absorption connective tissue and the beam-hardening effect.

WB is either immature or pathologic bone, with similar physical properties to soft tissues, unlike the lamellar bone. Therefore, for weak contrast, such as an unclear boundary due to low absorption coefficient, it is difficult to make an accurate standard in segmentation. Understanding the presence of WB in bone regeneration elucidates the BF potential. The approach to evaluating human-bone-biopsy specimens by high-energy X-rays from SR-μCT and the edge enhancement achieved by phase-contrast imaging resulted in an improved visualization and contrast of soft tissues such as WB. The edge enhancement provided by the phase-contrast method (Langer *et al.*, 2009; Betz *et al.*, 2007) and the depth of penetration provided by the SR-μCT images were sharper than the corresponding C-μCT images that had the same spatial resolution. Seo *et al.* (2015) previously investigated the ability of SR-μCT to evaluate NB formation in a human-bone-biopsy sample. Another study reported that a resolution of at least 4 μm is required to evaluate the bone structure (Palacio-Mancheno *et al.*, 2014; Bouxsein *et al.*, 2010). Indeed, the SR-μCT and C-μCT used in this work had similar spatial resolutions of ∼2 μm, and the number of projection images was 300 and 600, respectively. The edge-sharpening capability of SR-μCT allows it to depict the boundaries of NB, BS and WB. These improvements in visualization and sharpness are directly translated to the increased signal intensity contrast and the 1.5-fold increase illustrated in Fig. 4. Another possible explanation for this might be that higher-quality images can be obtained when images are acquired with the same projection number and pixel size as those in C-μCT.

The area and volume data were compared with the results of the C-μCT and SR-μCT analysis of the biopsy, using a similar region of interest (ROI). By using specific threshold settings (limit value = 50), SR-μCT was able to distinguish between NB, WB and grafted ROIs, and to gain insight into the 3D structure of the bone grown into the grafted maxillary sinus floor. Contrary to expectations, the C-μCT results did not exhibit a significant difference between the background and WB contrast values. The contrast value is the key parameter for the threshold segmentation. In this case, some pixels have intensity values below the threshold value, and some background pixels lie above the threshold value due to image inhomogeneities and additive noise. With C-μCT images, these pixels cannot be classified correctly because the contrast value adjacent to the background value is limited to the threshold setting. However, in phase-contrast imaging, the distance between the sample and the CCD camera can be adjusted, and there is a clear boundary with the structure due to the phase effect. It also provides improved contrast through image-filter processing. Thus, it is easy to set a threshold value using a clear boundary between the hard and soft tissues.

These results demonstrate two things. First, the observation region was limited to a field of view of 3 mm along the upper direction using SR-μCT; additional studies will be needed to

extend to a large field of view with collimation crystal optics. Second, it is necessary to study the NB formation process in the early stage of bone regeneration through an *in situ* experiment. Therefore, further studies will be needed to determine the low-dose exposure, fast scan and full field of view with high-resolution CT imaging.

5. Conclusions

This study demonstrated that for all the elements represented on grafted sites, clear and accurate segmentations resulted in realistic and detailed 3D images of WB structures such as NB and BS. SR-μCT can be used to improve the quality of visualization and analysis (NB, BS and WB) without the need for pre-processing of the sample. It also provides a remarkably high depiction of structural details and soft-tissue contrasts as well as higher CNRs than C-μCT. Threshold segmentations of NB, BS and WB structures are possible using these images and yield accurate reconstructions of 3D images. This SR-μCT tool and these threshold segmentations represent a promising development in high-quality-based segmentation methods for bone regeneration and remodeling.

Acknowledgements

The authors thank Jae-Hong Lim of the 6C beamline at the Pohang Accelerator Laboratory (Pohang, Republic of Korea) for his help during the experiments.

Funding information

This work was supported by a Biomedical Research Institute grant, Kyungpook National University Hospital (2017).

References

Betz, O., Wegst, U., Weide, D., Heethoff, M., Helfen, L., Lee, W. K. & Cloetens, P. (2007). *J. Microsc.* **227**, 51–71.
Bouxsein, M. L., Boyd, S. K., Christiansen, B. A., Guldberg, R. E., Jepsen, K. J. & Müller, R. (2010). *J. Bone Miner. Res.* **25**, 1468–1486.
Bushberg, J. T., Seibert, J. A., Leidholdt, E. M., Boone, J. M. & Goldschmidt, E. J. (2003). *Med. Phys.* **30**, 1936.
Finkemeier, C. G. (2002). *J. Bone Joint Surg. Am.* **84**, 454–464.
Froum, S. J., Wallace, S. S., Cho, S.-C., Elian, N. & Tarnow, D. P. (2008). *Int. J. Periodontics Restor. Dent.* **28**, 273–281.
Irie, M. S., Rabelo, G. D., Spin-Neto, R., Dechichi, P., Borges, J. S. & Soares, P. B. F. (2018). *Braz. Dent. J.* **29**, 227–238.
Jensen, O. T. & Sennerby, L. (1998). *Int. J. Oral Maxillofac. Implants*, **13**, 513–521.
John, H.-D. & Wenz, B. (2004). *Int. J. Oral Maxillofac. Implants*, **19**, 199–207.
Klein, M. O., Kämmerer, P. W., Götz, H., Duschner, H. & Wagner, W. (2013). *Int. J. Periodontics Restor. Dent.* **33**, e101–e110.
Kulak, C. A. M. & Dempster, D. W. (2010). *Arq. Bras. Endocrinol. Metab.* **54**, 87–98.
Langer, M., Prisby, R., Peter, Z., Boistel, R., Lafage-Proust, M.-H. & Peyrin, F. (2009). *Proceedings of the 31st Annual International Conference of the IEEE EMBS*, 2–6 September 2009, Minneapolis, MN, USA, pp. 1004–1007.
Martín-Badosa, E., Amblard, D., Nuzzo, S., Elmoutaouakkil, A., Vico, L. & Peyrin, F. (2003). *Radiology*, **229**, 921–928.
Moy, P. K., Lundgren, S. & Holmes, R. E. (1993). *J. Oral Maxillofac. Surg.* **51**, 857–862.
Palacio-Mancheno, P. E., Larriera, A. I., Doty, S. B., Cardoso, L. & Fritton, S. P. (2014). *J. Bone Miner. Res.* **29**, 142–150.
Raum, K., Hofmann, T., Leguerney, I., Saïed, A., Peyrin, F., Vico, L. & Laugier, P. (2007). *Bone*, **41**, 1017–1024.
Raven, C., Snigirev, A., Snigireva, I., Spanne, P., Souvorov, A. & Kohn, V. (1996). *Appl. Phys. Lett.* **69**, 1826–1828.
Schneider, P., Stauber, M., Voide, R., Stampanoni, M., Donahue, L. R. & Müller, R. (2007). *J. Bone Miner. Res.* **22**, 1557–1570.
Seo, S.-J., Bark, C. W., Lim, J.-H. & Kim, Y.-G. (2015). *Int. J. Nanomedicine*, **10**, 129–136.
Soardi, C. M., Clozza, E., Turco, G., Biasotto, M., Engebretson, S. P., Wang, H. L. & Zaffe, D. (2014). *Clin. Oral Implants Res.* **25**, 1161–1168.
Stelzle, F. & Benner, K. U. (2010). *Clin. Oral Implants Res.* **21**, 1370–1378.
Trisi, P., Rebaudi, A., Calvari, F. & Lazzara, R. J. (2006). *Int. J. Periodontics Restor. Dent.* **26**, 113–125.
Yildirim, M., Spiekermann, H., Handt, S. & Edelhoff, D. (2001). *Int. J. Oral Maxillofac. Implants*, **16**, 23–33.